Enhancing Permittivity of 3D Printing Filaments via Nanocompounding for Electromagnetic Applications

Bibek Kattel[†*], Utsab Ayan[‡], Madara Mohoppu[‡], Byron Villacorta[‡*], and Winn Elliott Hutchcraft[†*]
[†]Department of Electrical and Computer Engineering
[‡]Department of Chemical Engineering
[‡]Center for Graphene Research and Innovation
University of Mississippi
Oxford, MS, USA
[*]Email: {bkattel1, bsvillac, eeweh}@olemiss.edu

***Abstract*—This study explores the infusion of Calcium Copper Titanate nanoparticles into Acrylonitrile Butadiene Styrene (ABS) filament to enhance its permittivity for applications in the microwave (GHz) frequency range. The ABS and the nanoparticles were compounded at various concentrations to formulate nanocomposite filaments with 10wt%, 20wt%, and 40wt% nanoparticles. These nanocomposite filaments were used to 3D print test slabs designed to fit the WR137 waveguide to conduct permittivity measurement using reflection/transmission methods in a waveguide. Furthermore, the nanoparticles were characterized in the microwave (GHz) frequency range with the measurement of permittivity and dielectric loss using the waveguides. The results unveiled that the permittivity of the 3D printing filaments can be enhanced with the infusion of nanoparticle materials. This study provides valuable insights into the compounding process of the nanoparticles with ABS, offering a foundation for future development of nanocomposite filaments to advance additive manufacturing for electromagnetic applications.**

***Index Terms*—3D printing, Permittivity enhancement, ABS, Nanoparticles, Nanocomposite filaments, Characterization, Calcium copper titanate**

I. Introduction

Permittivity, often represented by relative permittivity or dielectric constant is a fundamental property that characterizes how a material polarizes in an electric field. Materials with higher permittivity have promising applications in the fields of microelectronics, electrical engineering, and biomedical engineering as reviewed in [1]. Higher permittivity materials could enhance electromagnetic shielding capabilities [2]. With a higher permittivity 3D printing filament, it may be possible to create 3D-printed enclosures or casings with improved electromagnetic interference (EMI) shielding properties and reflection loss, which are critical in electronics and telecommunications to prevent unwanted electromagnetic smog. In certain applications, achieving desired electromagnetic characteristics within small and compact devices is challenging. By enhancing the permittivity of the antenna substrate, it may be possible to miniaturize components while maintaining their electromagnetic performance as illustrated in various studies on the miniaturization of antennas [3]–[5]. In [6], [7], a linear relationship was demonstrated between effective relative permittivity and infill density in 3D printed slabs at microwave (GHz) frequencies. Hence, the availability of a higher permittivity material augments its versatility for a diverse array of applications in the GHz range. The same high permittivity filament material printed at different infill densities can be used for a variety of applications depending on the dielectric constant required for a specific application with an example of an optimized patch antenna for lower infill density substrate demonstrated in [8].

Numerous studies on nanocomposite filament formulation have characterized dielectric properties within the megahertz (MHz) frequency range [9]. However, with the widespread use of gigahertz (GHz) frequencies in modern devices, this study aims to investigate the dielectric properties of the nanocomposite material at the GHz frequency range. In [10], composite filaments for fused deposition modeling (FDM) 3D printing with ferroelectric barium titanate ($BaTiO_3$) micro-particles in an ABS matrix exhibited ε_r of 11 in the GHz range. In [11], the PLA filaments filled with graphene nanoplates and carbon nanotubes for FDM 3D printing have been evaluated. Their findings revealed variations in relative permittivity at the Ka-band, amounting up to 12.73, depending on filler percentage and processing method. A COC (Cyclic Olefin Copolymer) polymer loaded with titanium oxide (TiO_2) demonstrated high permittivity (up to 9.2) with low dielectric loss at 9.3 GHz, suitable for FDM as demonstrated in [5].

The development of tailored permittivity materials for microwave applications using fused filament fabrication (FFF) has been detailed in [12]. A flexible, high-dielectric constant composites using mixtures of polymer and ceramic nanoparticles ($BaTiO_3$, $SrTiO_3$, or $Ba_{0.67}Sr_{0.33}TiO_3$) was created and validated for effective medium approximations between 18 – 40 GHz. The measurement result shows a permittivity in the range of 4.10 to 8.39 for various concentrations of nanoparticles [12]. Additionally, [13] characterizes high-permittivity composite substrates based on Polydimethylsiloxane and Cyclo-Olefin Polymer matrices with $Ba_{0.55}Sr_{0.45}TiO_3$ and $MgCaTiO_2$ fillers up to 20 GHz. Their findings revealed ε_r ranging from 12.19 to 23.51, depending on micro-fillers concentration.

Amongst the plethora of studies on composite filaments for 3D printing applications, ABS stands out as a widely utilized

matrix material. Leveraging its well-documented performance in earlier studies, ABS has been chosen as the matrix material for this study. ABS exhibits notable strength and acceptable thermal shrinkage, expanding its suitability across various Fused Deposition Modeling (FDM) applications [14]. This thermoplastic amorphous polymer finds extensive use in FDM due to its dimensional stability and low glass transition temperature [15]. However, the relative permittivity of the ABS is relatively low for its wide applicability to be used as an antenna substrate.

Thus, the objective of this study is to improve the permittivity of the ABS filament by incorporating Calcium Copper Titanate ($CaCu_3Ti_4O_{12}$) nanoparticles (NPs) into it and produce a formulated filament material for 3D printing applications in the microwave (GHz) frequency range. The dielectric properties of these nanoparticles have not been thoroughly characterized in the GHz frequency range. This study aims to address this gap by characterizing the $CaCu_3Ti_4O_{12}$ NPs in the microwave (GHz) frequency range. These inorganic NPs were considered in this study due to their exceptional dielectric constant of about 10,286 and loss tangent of about 0.06712 when measured at 100 kHz [16]. The compounded filaments will subsequently serve as the base material for 3D printing WR137 waveguide slabs, enabling the characterization of the dielectric properties of the filament material within the microwave (GHz) frequency range with the waveguide measurement setup. The formulations developed are intended to boost the permittivity of the composite materials while ensuring minimal dielectric loss for radio frequency and antenna applications as well as retaining ABS filament processability for 3D printing applications.

II. Experimental

A. Manufacturing ABS Filament Prototype Without NPs

The initial phase of this study involved assessing the feasibility of extruding a 3D printing filament with ABS that meets the appropriate dimensional requirement of the 3D printer. The ABS material employed in this study was in pellet form sourced from McMasters with a Melt Flow Index of 35g/10min [17]. To manufacture the ABS filaments, the commercial pellets were dried under vacuum at 60°C for 2 hours to remove moisture prior to extrusion. The filaments were extruded in a Thermofisher Scientific PA11 Twin-screw extruder with L/D ratio of 40 with an 11-mm diameter screw customized with distributive and kneading elements and a selected temperature profile with settings for 10 different mixing zones. The extruded filaments were prepared and shaped into filaments using a 2.5 mm diameter circular die, a water bath to quench the filaments, followed up by a precise variable velocity take-up system to collect the extruded filaments as depicted in Fig. 1. The major extrusion parameters that yielded optimal filament production are listed in Table I.

The subsequent procedure entailed evaluating the printability of the extruded filament by feeding it to the 3D printer. The 3D printer employed in this study was a commercial 3Dn Series tabletop model manufactured by nScrypt which is a type of FDM printer. The filament material is forced into the nozzle of the 3D printer, where it is heated to its melting temperature using an integrated heater ring. Once heated, the filament material undergoes softening/melting and is extruded through an exceedingly narrow ceramic tip with an inner diameter of $125\,\mu m$ to enable layer-by-layer precise material deposition for the construction of intricate structures.

Fig. 1. Manufacturing process for the filaments via Twin-Screw Extrusion

A dielectric slab was fabricated as a test sample utilizing the 3D printer, which would subsequently be inserted into the WR137 waveguide for permittivity measurement. This waveguide has inner dimensions of 34.8488 mm x 15.7988 mm and the operating frequency range of this waveguide spans in the range of 5.85 GHz to 8.20 GHz. This waveguide was considered as it provided the right balance between the sample size and the useful frequency bands. The printing process as outlined in [8], [18] has been followed to print the test slabs fitting the WR137 waveguide using the 3D printer. The optimal settings that were utilized for 3D printing the test samples using the in-house ABS filament are listed in Table II with the 3D printed ABS test sample depicted in Fig. 2.

TABLE I
MANUFACTURING PARAMETERS OF THE FILAMENT

Parameter Name	Value
Extrusion speed	100 rpm
Temperature at feed zone	250°C
Temperature at the die	205°C
Back pressure at extruder	13-15 bar
Throughput	0.4 Kg/hr

TABLE II
3D PRINTING SETTINGS FOR ABS FILAMENT

Parameter Name	Value
Bed temperature	100°C
Nozzle temperature	250°C
Layer height	.350 mm
Extrusion width	.500 mm
Number of layers printed	23
Speed	30 mm/s
Infill pattern	Rectilinear
Infill density	100%

B. Compounding ABS with NPs

Following the successful utilization of the in-house ABS filaments in the fabrication of the test samples, the subsequent phase involved incorporating the $CaCu_3Ti_4O_{12}$ nanoparticles (NPs) into the ABS base polymer. The $CaCu_3Ti_4O_{12}$ nanoparticles, procured from Matexcel had a purity of 99.5% and a particle size of approximately $360\,\mathrm{nm}$ [19]. It is important to acknowledge that this study relied on the specifications provided by the supplier, as a comprehensive evaluation of the acquired NPs was beyond the study's purview.

The NPs were incorporated via melt-mixing using a similar process to that of the extrusion of the ABS filaments using the twin extruder, the water bath, and the take-up unit. The dried ABS pellets were fed using a continuous volumetric screw feeder (Conair TrueFeedTM with a GLX metering cylinder), and the NPs were independently fed using a vibratory feeder (Syntron Vib F-TO) at relative rates to that of the ABS pellets as to produce the desired concentrations. The NPs were added at 10, 20, and 40 wt% nominal compositions to assess the effect of concentration on the permittivity of the nanocomposite filament material. These nanocomposite filaments were subsequently fed into the 3D printer to manufacture test samples for the WR137 waveguide using the same print settings employed for ABS. While the same settings proved effective for the 10% and 20% NPs filaments, some adjustments were necessary for the 40% NPs filament due to the increased viscosity generated by the NPs at such a high loading fraction. Specifically, the temperature had to be elevated to nearly 300°C to facilitate printing. Nonetheless, challenges were encountered during the printing of the 40% NPs filament, resulting in noticeable ridges and surface irregularities in the printed layers. This suggests that the addition of nanoparticles may have compromised some of the ABS's 3D printing characteristics (i.e., viscosity and mechanical properties). The fabricated test slabs using the 10%, 20%, and 40% NPs filaments are depicted in Fig. 3.

(a) cross sectional view

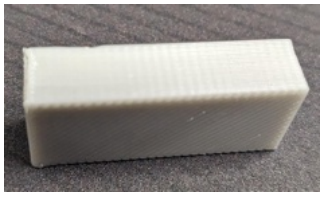

(b) isometric view

Fig. 2. 3D printed test sample fabricated with in-house ABS filament

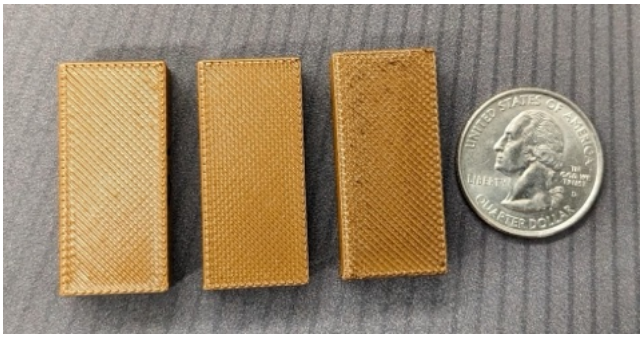

Fig. 3. Test slabs fabricated with nanocomposite filaments with 10wt%, 20wt%, and 40wt% NPs (left to right)

III. MEASUREMENT OF THE DIELECTRIC CONSTANT

The ensuing phase in this study entails quantifying the relative permittivity of the test slabs fabricated with additive methods. These test samples include the 3 nano-compounded test slabs along with the test slab fabricated with the in-house ABS filament. This assessment seeks to discern the impact of nanoparticles integration on the relative permittivity of the nanocomposite filament. Thus, it is imperative to conduct precise permittivity measurements on these WR137 test slabs. For this purpose, a measurement setup using a WR137 waveguide calibrated with Agilent PNA-X Vector Network Analyzer was utilized. The waveguide was calibrated using a TRL (Thru-Reflect-Line) calibration method [20], before any measurements following a setup and process as described in [6]. The following 3 measurement models available in the 85071E PNA X were utilized for the measurement of ε_r and μ_r of the 3D printed slabs: (i) Reflection / Transmission Mu and Epsilon Polynomial Fit (ii) Reflection / Transmission Epsilon Precision, and (iii) Transmission Epsilon Fast [21], [22]. Despite assuming both the NPs and ABS to be non-magnetic, at least one method capable of measuring both the permittivity and permeability of the 3D printed test slabs was employed to ensure certainty. The 3 models along with their alternate names and measurement outcomes have been listed in Table III.

IV. RESULTS

The waveguide method provided results for various frequencies across its operating range. Fig. 4 and 5 illustrate the permittivity measurements of the 20% and 40% nanocomposite

TABLE III
MEASUREMENT MODELS USED

85071E name	Alternate Name	Result/s	Reference
(i)	Poly Fit	ε_r , μ_r	[23]
(ii)	NIST Precision	ε_r (μ_r=1)	[24]
(iii)	Fast Transmission	ε_r (μ_r=1)	unpublished [21]

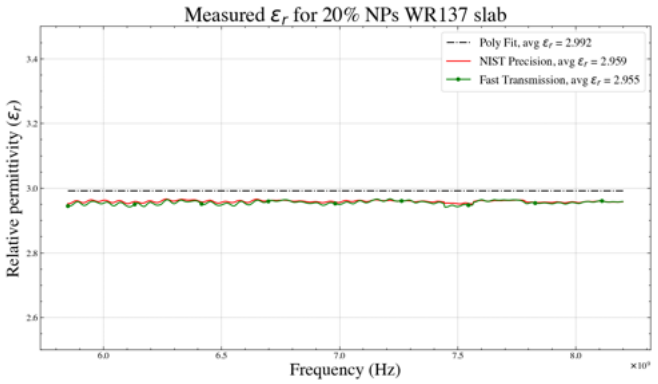

Fig. 4. Measured ε_r for 20% NPs slab using different methods.

TABLE IV
MEASUREMENT RESULTS FOR VARIOUS WR 137 SLABS

Slab Name	(i)	(ii)	(iii)
ABS only	2.34	2.34	2.33
10% NPs	2.38	2.39	2.38
20% NPs	2.99	2.96	2.96
40% NPs	4.27	4.13	4.12

TABLE V
PERCENTAGE INCREASE IN RELATIVE PERMITTIVITY COMPARED TO ABS

Slab Name	(i)	(ii)	(iii)
10% NPs	1.71	2.14	2.15
20% NPs	27.78	26.50	27.04
40% NPs	82.48	76.50	76.82

test slabs, respectively, across the operating frequency range of the WR137 waveguide. However, for effective comparison, we sought a single permittivity value for each slab. To achieve this, we averaged the data obtained for different frequencies as it exhibited minimal variation across the measured span of frequencies. The resulting averaged permittivity values for the slabs are presented in Table IV. Additionally, the percentage increment in relative permittivity of the nanocomposite slabs compared to the ABS slabs has been presented in Table V. The average dielectric loss of these nanocomposite test slabs varied between 0.002228 and 0.004163 indicating low loss characteristics for radio frequency applications.

A. *Characterization of $CaCu_3Ti_4O_{12}$ at GHz range*

The exceptionally high permittivity exhibited by the NPs in the KHz frequency range did not materialize in the nanocomposite test slabs when measured at the GHz frequency range. Consequently, a direct assessment of the permittivity of the NPs was conducted. This was achieved by compactly filling WR90 and WR62 sample holders with the NPs. These holders, loaded with NPs were subsequently inserted into respective waveguides for permittivity measurement. The WR90 waveguide spans the frequency range from 8.2 to 12.4 GHz, while the WR62 extends from beyond 12.4 to 18 GHz. The results of the NPs permittivity measurements, conducted using both waveguides, are depicted in Fig. 6. The plot depicts two solid lines representing measurements conducted with the WR90 waveguide, with corresponding frequencies displayed on the bottom horizontal axis. Additionally, two dashed/dotted lines represent measurements using the WR62 waveguide, and their respective frequencies are listed on the top horizontal axis. Notably, two distinct measurement techniques were employed, as outlined in the figure legend. The average permittivity values obtained for the NPs using the WR90 sample holder were 8.87 and 8.88 using the Poly Fit method and Fast Transmission method, respectively. Similarly, the average permittivity values for the NPs using the WR62 sample holder were 9.70 and 9.66 for the Poly Fit and Fast Transmission methods, respectively. Also, the dielectric loss of the nanoparticles material was found to be in the range of 0.0033-0.0057 across both measurement bands indicating it possesses low dielectric loss characteristics at microwave frequencies.

V. DISCUSSION

The results presented in Tables IV and V highlight a notable increase in the relative permittivity of the nanocomposite test slabs, particularly evident in the cases of 20% and 40% nanoparticle content. Specifically, the nanocomposite test slab

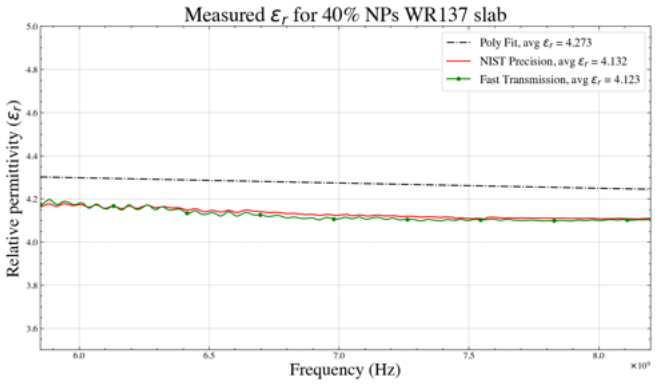

Fig. 5. Measured ε_r for 40% NPs slab using different methods.

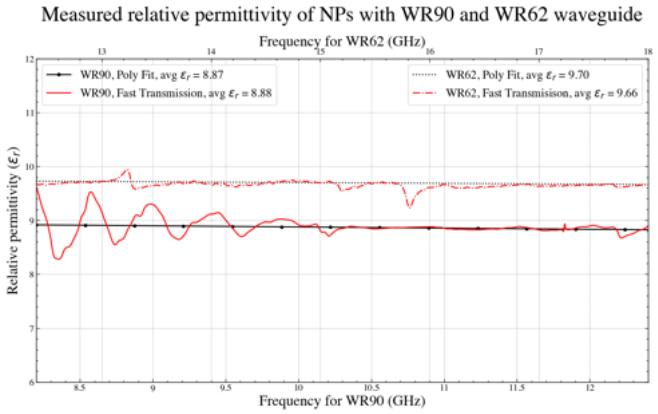

Fig. 6. Measured ε_r of the NPs using WR90 and WR62 waveguide.

with 40% NPs content displayed a substantial increase in permittivity, amounting to at least 76% improvement. This outcome holds immense promise for ongoing research, especially with the promising applications of these 3D printing nanocomposite filament materials for radio frequency and antenna design. Unexpectedly, incorporating 10% NPs into the nanocomposite slab had little effect on its relative permittivity. This could be attributed to the error in the initial filament mixing process, potentially leading to a lower than intended nanoparticles concentration within the 10% NPs filament batch.

Another significant aspect of this study is the characterization of Calcium Copper Titanate nanoparticles within the GHz frequency range. Interestingly, it was observed that the relative permittivity of the nanoparticles in this frequency range was not exceptionally high, unlike observed at the 100 kHz frequency ranges as documented in [16]. This finding, illustrated in Fig. 6, elucidates why achieving a high permittivity 3D printing filament for GHz operations is challenging, especially considering the limited characterization of nanoparticles within the GHz range. Nevertheless, this study provides valuable insights into nanoparticles behavior undergoing significant variations in dielectric properties across different frequency ranges.

Moreover, it became evident that there are limitations to the extent of nanoparticles addition to the ABS material, as higher nanoparticles content compromised the 3D printability of ABS. Notably, the 40% NPs filament exhibited increased brittleness, affecting the mechanical properties of the manufactured test slab. However, mechanical tests were not performed due to project limitations, despite indications of potential mechanical property deterioration. Further research is warranted to explore the relationship between nanoparticle content and the mechanical properties of the nanocomposite filament. Despite these challenges, ABS remains a robust matrix material for nanoparticles integration, particularly with lower nanoparticle content. The addition of the nanoparticles up to 40% NPs content in the 3D printing filaments, despite associated issues, indicates the compatibility of ABS as a matrix material.

An essential takeaway from this study is the viability of the proposed permittivity enhancement technique. Although the nanoparticles themselves did not exhibit very high permittivity within the GHz frequency range, the approach remains effective. This suggests that with the formulation of nanoparticles possessing high permittivity within the GHz frequency range, the development of high-permittivity 3D printing filaments for GHz applications becomes a tangible possibility. This avenue holds substantial potential for advancing the capabilities of 3D printed substrates in electrical engineering and beyond.

VI. Conclusions

In summary, the incorporation of NPs successfully augmented the permittivity of the ABS filament. The results, particularly the 20% and 40% nanoparticle content, showed promising results. Furthermore, this study reaffirms ABS as an outstanding matrix for nanoparticle integration. Furthermore, the dielectric properties of Calcium Copper Titanate nanoparticles were characterized within the GHz frequency range. Future research endeavors will explore various nanoparticles, assessing their dielectric properties within the GHz range as well as their ability to be compounded with commercial 3D printing filaments. This exploration would advance the development of filaments with higher dielectric constants. This research highlights the potential of nanoparticle integration in 3D printing filaments to enhance dielectric properties, broadening the applicability of 3D-printed materials. The insights gained from this study serve as a valuable foundation for future progress in the realm of dielectric materials and their applications.

Acknowledgment

This work was supported in part by Raytheon Co. and the NSF Industry University Cooperative Research Centers under Grant 1822104. We would like to acknowledge the use of Matplotlib and SciencePlots [25] for generating the plots in this paper.

References

[1] Z.-M. Dang, J.-K. Yuan, J.-W. Zha, T. Zhou, S.-T. Li, and G.-H. Hu, "Fundamentals, processes and applications of high-permittivity polymer–matrix composites," *Progress in Materials Science*, vol. 57, no. 4, pp. 660–723, May 2012, ISSN: 00796425. DOI: 10.1016/j.pmatsci.2011.08.001.

[2] Q. Qin, Y. Hu, S. Guo, *et al.*, "PVDF-based composites for electromagnetic shielding application: A review," *Journal of Polymer Research*, vol. 30, no. 3, p. 130, Mar. 9, 2023, ISSN: 1572-8935. DOI: 10.1007/s10965-023-03506-y.

[3] N. Altunyurt, M. Swaminathan, P. M. Raj, and V. Nair, "Antenna miniaturization using magneto-dielectric substrates," in *2009 59th Electronic Components and Technology Conference*, May 2009, pp. 801–808. DOI: 10.1109/ECTC.2009.5074103.

[4] M. Boudjerda, A. Reddaf, A. Kacha, *et al.*, "Design and Optimization of Miniaturized Microstrip Patch Antennas Using a Genetic Algorithm," *Electronics*, vol. 11, no. 14, p. 2123, Jan. 2022, ISSN: 2079-9292. DOI: 10.3390/electronics11142123.

[5] R. Czarny, T. Q. V. T. Q. Hoang, B. Loiseaux, *et al.*, "High Permittivity, Low Loss, and Printable Thermoplastic Composite Material for RF and Microwave Applications," in *2018 IEEE Conference on Antenna Measurements & Applications (CAMA)*, 2018, pp. 1–4. DOI: 10.1109/CAMA.2018.8530660.

[6] B. Kattel, W. Hutchcraft, and R. Gordon, "Experimental verification of simulation model for permittivity of 3D-printed slabs with various infill densities," *(preprint) TechRxiv*, 2023. DOI: 10.36227/techrxiv.23661705.v1.

[7] B. Kattel, W. E. Hutchcraft, and R. K. Gordon, "Exploring infill patterns on varying infill densities on dielectric properties of 3D printed slabs," *2023 Antenna Measurement Techniques Association Symposium (AMTA)*, pp. 1–5, 2023. DOI: 10.23919/AMTA58553.2023.10293640.

[8] B. Kattel, W. E. Hutchcraft, and R. K. Gordon, "3D printed patch antennas with varying infill densities," *2023 Antenna Measurement Techniques Association Symposium (AMTA)*, pp. 1–5, 2023. DOI: 10.23919/AMTA58553.2023.10293739.

[9] W. H.-Y. Clarissa, C. H. Chia, S. Zakaria, and Y. C.-Y. Evyan, "Recent advancement in 3-D printing: Nanocomposites with added functionality," *Progress in Additive Manufacturing*, vol. 7, no. 2, pp. 325–350, 2022. DOI: 10.1007/s40964-021-00232-z.

[10] Y. Wu, D. Isakov, and P. S. Grant, "Fabrication of composite filaments with high dielectric permittivity for fused deposition 3D printing," *Materials*, vol. 10, no. 10, p. 1218, 2017. DOI: 10.3390/ma10101218.

[11] R. Adami, P. Lamberti, D. Bychanok, P. Kuzhir, and V. Tucci, "Electromagentic properties of filaments containing nanofillers for 3D printing," 2021. DOI: 10 . 3303 / CET2184019.

[12] P. Parsons, Z. Larimore, M. Mirotznik, and G. Mitchell, "Composite materials development for fused filament fabrication of RF systems," in *2020 International Applied Computational Electromagnetics Society Symposium (ACES)*, 2020, pp. 1–2. DOI: 10.23919/ACES49320.2020.9196124.

[13] J. Castro, E. Rojas, T. Weller, and J. Wang, "Engineered Nanocomposites for Additive Manufacturing of Microwave Electronics," *International Symposium on Microelectronics*, vol. 2015, no. 1, pp. 000 189–000 196, Oct. 2015, ISSN: 1085-8024. DOI: 10.4071/isom-2015-WA12.

[14] S. K. Selvamani, M. Samykano, S. R. Subramaniam, *et al.*, "3D printing: Overview of ABS evolvement," Kuantan, Malaysia, 2019, p. 020 041. DOI: 10.1063/1.5085984.

[15] A. R. Torrado Perez, D. A. Roberson, and R. B. Wicker, "Fracture Surface Analysis of 3D-Printed Tensile Specimens of Novel ABS-Based Materials," *Journal of Failure Analysis and Prevention*, vol. 14, no. 3, pp. 343–353, Jun. 1, 2014, ISSN: 1864-1245. DOI: 10.1007/s11668-014-9803-9.

[16] M. Subramanian, D. Li, N. Duan, B. Reisner, and A. Sleight, "High Dielectric Constant in ACu3Ti4O12 and ACu3Ti3FeO12 Phases," *Journal of Solid State Chemistry*, vol. 151, no. 2, pp. 323–325, May 2000, ISSN: 00224596. DOI: 10.1006/jssc.2000.8703.

[17] McMaster-CARR. "ABS specifications." (Nov. 1, 2023), [Online]. Available: https://www.mcmaster.com/4387N11/.

[18] C. D. Keathley, "Evaluation of manufacturing methods for antenna design," M.S. thesis, The University of Mississippi, 2021.

[19] Matexcel. "CaCu3Ti4O12 Nano Powder." (Nov. 1, 2023), [Online]. Available: https://www.matexcel.com/calcium-copper-titanate-cacu3ti4o12-nano-powder-item-1261.html.

[20] Keysight Technologies. "TRL calibration." (Nov. 15, 2023), [Online]. Available: https://rfmw.em.keysight.com/wireless/helpfiles/pxivna/S3_Cals/TRL_Calibration.htm.

[21] Agilent. "Models in The 85071E Materials Measurement Software," Scribd. (Nov. 15, 2023), [Online]. Available: https://www.scribd.com/document/562103233/85071-e-Models.

[22] Keysight, "85071E Materials Measurement Software," 2014. [Online]. Available: https://www.keysight.com/us/en/assets/7018-01155/technical-overviews/5988-9472.pdf.

[23] P. G. Bartley and S. B. Begley, "A new technique for the determination of the complex permittivity and permeability of materials," in *2010 IEEE Instrumentation & Measurement Technology Conference Proceedings*, 2010, pp. 54–57. DOI: 10.1109/IMTC.2010.5488184.

[24] J. Baker-Jarvis, E. Vanzura, and W. Kissick, "Improved technique for determining complex permittivity with the transmission/reflection method," *IEEE Transactions on Microwave Theory and Techniques*, vol. 38, no. 8, pp. 1096–1103, 1990. DOI: 10.1109/22.57336.

[25] J. D. Garrett, "garrettj403/SciencePlots," version 1.0.9, Sep. 2021. DOI: 10.5281/zenodo.4106649.